AFRL-RV-PS-
TR-2014-0002

UNDERSTANDING THE EFFECTS OF ENERGY FROM THE SOLAR WIND TO THE MAGNETOSPHERE IONOSPHERE-THERMOSPHERE SYSTEM

Christos Christodoulou

Department of Electrical and Computer Engineering
University of New Mexico
Albuquerque, NM 87131

29 August 2013

Final Report

AIR FORCE RESEARCH LABORATORY
Space Vehicles Directorate
3550 Aberdeen Ave SE
AIR FORCE MATERIEL COMMAND
KIRTLAND AIR FORCE BASE, NM 87117-5776

DTIC COPY

NOTICE AND SIGNATURE PAGE

Using Government drawings, specifications, or other data included in this document for any purpose other than Government procurement does not in any way obligate the U.S. Government. The fact that the Government formulated or supplied the drawings, specifications, or other data does not license the holder or any other person or corporation; or convey any rights or permission to manufacture, use, or sell any patented invention that may relate to them.

This report was cleared for public release by the 377 ABW Public Affairs Office and is available to the general public, including foreign nationals. Copies may be obtained from the Defense Technical Information Center (DTIC) (http://www.dtic.mil).

AFRL-RV-PS-TR-2014-0002 HAS BEEN REVIEWED AND IS APPROVED FOR PUBLICATION IN ACCORDANCE WITH ASSIGNED DISTRIBUTION STATEMENT.

//SIGNED//	//SIGNED//
Dr. Daniel Ober	Edward J. Masterson, Colonel, USAF
Program Manager/RVBXP	Chief, Battlespace Environment Division

This report is published in the interest of scientific and technical information exchange, and its publication does not constitute the Government's approval or disapproval of its ideas or findings.

REPORT DOCUMENTATION PAGE

Form Approved
OMB No. 0704-0188

1. REPORT DATE *(DD-MM-YYYY)*	**2. REPORT TYPE**	**3. DATES COVERED** *(From - To)*
29-08-2013	Final Report	29 Feb 2012 – 29 May 2013

4. TITLE AND SUBTITLE
Understanding the Effects of Energy from the Solar Wind to the Magnetosphere Ionosphere-Thermosphere System

5a. CONTRACT NUMBER
FA9453-12-1-0171

5b. GRANT NUMBER

5c. PROGRAM ELEMENT NUMBER
61102F

6. AUTHOR(S)
Christos Christodoulou

5d. PROJECT NUMBER
3001

5e. TASK NUMBER
PPM00017357

5f. WORK UNIT NUMBER
EF121211

7. PERFORMING ORGANIZATION NAME(S) AND ADDRESS(ES)
Department of Electrical and Computer Engineering
University of New Mexico
Albuquerque, NM 87131

8. PERFORMING ORGANIZATION REPORT NUMBER

9. SPONSORING / MONITORING AGENCY NAME(S) AND ADDRESS(ES)
Air Force Research Laboratory
Space Vehicles Directorate
3550 Aberdeen Avenue SE
Kirtland AFB, NM 87117-5776

10. SPONSOR/MONITOR'S ACRONYM(S)
AFRL/RVBXP

11. SPONSOR/MONITOR'S REPORT NUMBER(S)
AFRL-RV-PS-TR-2014-0002

12. DISTRIBUTION / AVAILABILITY STATEMENT

Approved for Public Release: distribution is unlimited. (377ABW-2014-0074 dtd 10 Feb 2014)

13. SUPPLEMENTARY NOTES

14. ABSTRACT

Recent studies have shown that sudden enhancement of solar wind dynamic pressure (Psw) is a significant driver of energy transfer to the magnetosphere-ionosphere (MI) system, generating strong responses such as increase in the cross polar cap potential (CPCP), reduction of the polar cap area, expansion of the auroral oval, etc. This study investigates where, when, and how solar wind energy is deposited into the MI system during sudden solar wind dynamic pressure enhancement, like shocks. We analyze three unique events that occurred during strongly southward, near-zero Bz, and northward IMF by simulating the MI responses with the OpenGGCM coupled magnetosphere-ionosphere-thermosphere model. We examine the behavior of dayside and nightside reconnection, and quantify their respective contribution to CPCP, a proxy of ionospheric flow convection.

15. SUBJECT TERMS
Solar wind, Magnetosphere, Thermosphere, Ionosphere, Dayside and nightside reconnection

16. SECURITY CLASSIFICATION OF:			**17. LIMITATION OF ABSTRACT**	**18. NUMBER OF PAGES**	**19a. NAME OF RESPONSIBLE PERSON**
a. REPORT	**b. ABSTRACT**	**c. THIS PAGE**	Unlimited	32	Dr. Daniel Ober
Unclassified	Unclassified	Unclassified			**19b. TELEPHONE NUMBER** *(include area code)*

This page is intentionally left blank.

TABLE of CONTENTS

LIST OF FIGURES

1. INTRODUCTION

Interplanetary Magnetic Field (IMF) condition is an well-known driver that flows solar wind energy into the magnetosphere-ionosphere (MI) system, causing strong geomagnetic events such as magnetic storms and substorms. In addition to the IMF condition, recent studies [Zesta et al., 2000; Boudouridis et al., 2004a, 2004b, 2005, 2007, 2008a, 2008b, 2011] showed that sudden enhancements of solar wind dynamic pressure (Psw) derives intense magnetosphere-ionosphere interactions, suggesting that the Psw enhancement can be a significant driver to deposit solar wind energy into the MI system. The well-known MI responses include increase of cross-polar-cap ionospheric potential (CPCP), polar cap area closure, fast ionospheric flows, and auroral oval broadening.

These MI interactions during the sudden Psw enhancements indicate a strong relation to magnetic reconnection that happens in both of the dayside and nightside magnetosphere. Boudouridis et al. [2007, 2011] showed from Super Dual Auroral Radar Network (SuperDARN) observations that the dayside ionospheric convection significantly increases about four minutes after the arrival of Psw fronts. These fast plasma flows are observed in the vicinity of magnetic foot prints that are connected to the expected reconnection sites on the dayside magnetopause. This indicates that the Psw enhancement initiates active magnetopause reconnection.

The Psw increase also enhances the magnetotail reconnection. The particle precipitation data from Defense Meteorological Satellite Program (DMSP) and Polar Ultra Violet Imager (UVI) [Lyons, 2000; Zesta et al., 2000; Milan et al., 2004; Hubert et al., 2006, 2009; Boudouridis et al. 2003, 2004a, 2008b] showed that the polar cap area shrinks mostly on the nightside after the Psw increase. This means reduction of open magnetic flux in the nightside magnetosphere, i.e., increase of reconnection rate in the central plasma sheet. The SuperDARN observations [Boudouridis et al., 2011] also showed fast plasma flows on the nightside ionosphere about 10 – 15 minutes after the arrival of Psw increase, suggesting strong magnetotail reconnection during the Psw enhancements.

The previous studies provide clear evidences that the increase of solar wind dynamic pressure activates both dayside and nightside reconnection. However, the following fundamental questions are still unanswered: how the reconnection rates vary throughout the Psw enhancement, which physical process causes increase of reconnection rates, and how strongly

they contribute to the ionospheric convection enhancement. This paper investigates the answers using a 3D global magnetosphere – ionosphere - thermosphere model called Open Geospace General Circulation Model – Coupled Ionosphere Thermosphere Model (OpenGGCM-CTIM).

For the model studies, we select three unique events of sudden Psw enhancements during negative, near-zero, and positive IMF Bz. These events have been thoroughly investigated in the previous studies [Zesta et al., 2000; Boudouridis et al., 2003, 2011] using DMSP, SuperDARN, and Polar UVI Imagers. Therefore, these observations are available for the model validation as well as for the further detailed studies. We input solar wind conditions of the three events into the OpenGGCM-CTIM model, and simulate their magnetosphere-ionosphere responses. The model reproduces increase of CPCP, polar cap closure, and enhancements of ionospheric flows to a reasonable extent, showing a good agreement with the observations.

With these model results, we investigate the behaviors of dayside and nightside reconnection during the three different events, and estimate the relative importance of each merging rate on the ionospheric convection. The dayside and nightside reconnection rates are determined to be the changes of open flux per unit time crossing the dayside and nightside Open-Closed field line Boundary (OCB). The activity of ionospheric convection is estimated in terms of cross polar cap potential. Then, we fit the reconnection rates and CPCP from OpenGGCM-CTIM to a well known equation of the Expanding and Contracting Polar Cap (ECPC) model, $CPCP = C_d\Phi_d + C_n\Phi_n + \Phi_v$. The Φ_d, Φ_n, and Φ_v are electric voltages resulted from dayside reconnection, nightside reconnection, and viscosity interaction. The C_d and C_n are regression coefficients which determines quantitative contribution of each merging rate on CPCP increase, i.e., enhancement of ionospheric convection.

This study answers when, where, and how solar wind energy is deposited into the magnetosphere-ionosphere system during the sudden enhancement of solar wind dynamic pressure. The detailed methodology is discussed in section 2. Section 3 explains the dayside and nightside reconnection patterns of the three events. The relation between the reconnection rates and the CPCP are discussed in section 4. Finally, section 5 summarizes our results.

2. METHODOLOGY

2.1 OpenGGCM-CTIM model

We use OpenGGCM-CTIM, a 3D coupled magnetosphere – ionosphere - thermosphere model, in order to simulate the magnetosphere-ionosphere responses to the sudden enhancements of solar wind dynamic pressure. This model divides the Earth's geospace system into two regions (the magnetosphere and MI coupling zone), and applies different calculation strategies based on the main physical process of each region.

OpenGGCM calculates plasma behaviors of the magnetosphere region by solving resistive MHD equations as initial-boundary-value problems. Inner boundary of the magnetosphere is located at 3 – 4 Re from the Earth, and its outer boundary extends to the OpenGGCM simulation box. X range of the simulation box is from 20 – 30 Re sunward to 600 – 2000 Re anti-sunward, and its YZ range is -48 – 48 Re. Thus, the simulation box is spacious enough to cover the magnetosphere and its surrounding environments such as bow shock and magnetosheath. The numerical grids are non-uniform Cartesian grids and densely located near the dayside magnetosphere and near Ygse=Zgse=0, where magnetic reconnection is expected to occur. OpenGGCM uses solar wind conditions from ACE, WIND, or Geotail spacecraft as input, and provides number density, velocity, plasma pressure, and electromagnetic fields as output.

OpenGGCM and CTIM calculate dynamics of MI couping zone. OpenGGCM derives an ionospheric potential equation as a function of Field Aligned Currents (FACs) and ionospheric conductance by assuming that the FACs generated from the solar wind – magnetosphere interaction should be closed in the ionosphere. To calculate electric potentials, OpenGGCM obtains FACs from the inner boundary of the magnetosphere, and maps them to the ionosphere along the dipole magnetic field lines. Ionospheric conductance is obtained from CTIM. This model self-consistently solves both neutral and ion fluid equations from 80 km to several 1000 km in altitude, providing realistic ionospheric conductance to OpenGGCM. Finally, OpenGGCM maps the obtained electric potentials back to the inner boundary of the magnetosphere, and uses them to estimate the magnetospheric plasma flows. More detailed information about the OpenGGCM and CTIM models can be found in Raeder et al. [2001, 2003, 2008] and Fuller-Rowell et al. [1996].

2.2 Reconnection rates

We apply the method of Ober et al. [2007] to calculate reconnection rates. The dayside and nightside reconnection rates (Φ_d and Φ_n) are defined to be the open flux per unit time crossing the dayside and nightside open-closed field line boundary. Therefore,

$$\Phi = \int (\boldsymbol{V_b} - \boldsymbol{V_p}) \times \boldsymbol{B} \cdot d\boldsymbol{l} \quad (1)$$

where $d\boldsymbol{l}$ is an infinitesimal distance along OCB, $\boldsymbol{V_b}$ a normal velocity of OCB, and $\boldsymbol{V_p}$ a velocity of the ionospheric plasma flow perpendicular to the OCB. The $\boldsymbol{V_b} \times \boldsymbol{B}$ term represents the electric potential caused by the motion of OCB, while the $\boldsymbol{V_p} \times \boldsymbol{B}$ term indicates electrostatic potentials resulted from ionospheric flows. Thus, the reconnection rate is the difference between the two electric potentials. This method is basically the same method used to calculate reconnection rates with the observation data [de La Beaujardiere et al., 1991; Blanchard et al., 1996; Ober et al., 2001; Ober et al, 2007].

To calculate OCB, we trace magnetic field lines from every ionospheric grid points through the magnetosphere. The grid resolution is 3°× 0.5° in magnetic longitude and latitude. We stop the tracing when the field line enters a sphere of radius 4 Re, when it reaches a model simulation box, or when its length becomes 1,000 Re. The first field line is considered as being closed, and the last two are considered as being open. We mark the ionospheric grids connected to closed and open field lines with -1 and 1, respectively. The zero contour of those grids are OCB. To determine the dayside and nightside portions of OCB, we obtain ionospheric electric potentials along OCB from OpenGGCM-CTIM. The region from maximum to minimum potentials is considered as a dayside OCB, and the rest is a nightside OCB. We determine the OCB as well as its dayside/nightside portion at every minutes, applying the results to calculate the one-minute reconnection rates.

2.3 CPCP fitting

To understand the contribution of reconnection rates to CPCP, we fit the reconnection rates and modeled CPCP to a widely used linear function from Expanding-Contracting Polar Cap Model [Lockwood et al. 2009 and references therein] :

$$\Phi_{cpcp} = C_d \Phi_d + C_n \Phi_n + \Phi_v \quad (2)$$

where Φ_{cpcp} is cross polar cap ionospheric potential, Φ_v is the viscous-like potential contribution,

and C_d (C_n) is a regression coefficient of dayside (nightside) merging rates. The Φ_v is defined to be CPCP minus the potential different along OCB. The regression coefficients can be considered as a weight factor, estimating the quantitative contribution of reconnection rates to CPCP during sudden Psw increase.

3. CASE STUDIES

3.1 10 January 1997

The first event happens during the moderate geomagnetic storm on January 10 1997. At the end of main phase, solar wind pressure increases from 2 to 6 nPa for 20 minutes while IMF remains stationary. IMF, solar wind speed, number density, and dynamic pressure of this event are shown in the top four panels of Figure 1. The vertical black line represents when pressure shock arrives at the magnetopause nose. The previous studies [Lyons, 2000; Zesta et al., 2000; Boudouridis et al., 2003; Boudouridis et al., 2004a] have observed auroral oval expansion, polar cap closing, enhanced CPCP, and fast ionospheric flows in the polar cap and auroral ovals during this pressure enhancement .

We simulate the magnetosphere - ionosphere responses of this event by inputing the solar wind parameters in Figures 1.a – 1.e into the OpenGGCM-CTIM model. The modeled polar cap area and CPCP are shown in Figure 1.f and 1.e. The blue line and red dots in Figure 1.e represent the CPCPs obtained from our model and DMSP spacecraft, respectively. Polar cap area expands at ~11:00 UT for several minutes, and shrinks continuously until solar wind dynamic pressure slightly increases from 0.5 to 2 nPa at 11:30 UT. The polar cap closure is also observed by Polar UVI Images [Lyons, 2000; Zesta et al., 2000] and DMSP particle fluxes [Boudouridis et al., 2003]. The modeled CPCP increases from 140 to 200 kV, and the DMSP CPCP enhances from 120 to 220kV. The magnitude and jump scale of both CPCPs generally match. However, our model reduces CPCP faster after the first Psw jump, and maintain it at a little higher value after the second pressure increase. In spite of this difference, the OpenGGCM-CTIM reasonably generates the well-known ionospheric responses (polar cap closure and CPCP increase) to Psw enhancements.

We employ the method in section 2.2 to calculate dayside and nightside reconnection rates (Φ_D and Φ_N) of OpenGGCM-CTIM. These results are shown in Figure 1.g. The dayside

reconnection rate reacts first to the Psw enhancement, and increases from 60 kV to 160 kV in a few minutes after the shock. The nightside reconnection rate reaches its maximum at 11:09 UT, about 9 minutes later than the time of the maximum dayside reconnection rate. This nightside reconnection dominates until the second pressure pulse strengthens the dayside reconnection at 11:27 UT.

We plot the magnetosheath fields in Figure 1.h in order to investigate the dayside reconnection mechanisms during strong solar wind pressure. The magnetosheath fields were obtained at the location 1 Re sunward from the magnetopause nose. While IMF remains steady, total field magnitude (black line) of the magnetosheath increases up to 85 nT during the first pressure shock. The field strength drops quickly after the shock, and enhances again during the small increase of Psw at 11:27 UT. The pressure shock compresses the magnetosheath and intensifies its magnetic fields. The stronger magnetosheath fields are draped over the dayside magnetopause. This initiates more active anti-parallel reconnection, thus increasing the dayside reconnection rate.

Note a good correlation between the dayside reconnection rate and the magnetosheath field strength although the calculation of reconnection rate does not need the fields as a parameter. Several modeling studies [Borovsky et al., 2008] have predicted the strong relation between the dayside reconnection and the magnetosheath fields, and selected the field information as a major parameter to calculate the reconnection rate. The stronger the magnetosheath fields are, the higher the dayside reconnection rate is. We calculate the reconnection rate without the magnetosheath field, and observe the close relation between the two parameters. Our model results confirm the previous modeling predictions.

Figure 2 displays how the magnetosphere changes in a response to the Psw shock. Dynamic pressure (Pdy), X component of velocity (Vx), total magnetic field (Bt), and X component of magnetic field (Bx) on the noon-midnight meridian plane are plotted every 10 minutes during 10:50 – 11:30 UT. The first column shows the magnetosphere at 10:50 UT before the shock arrival. We observe the preexisting nightside reconnection near Xgse=-20 Re with a strong earthward plasma flow. At 11:00 UT, the pressure shock hits the dayside magnetopause, and the bow shock nose moves to Xgse = 11 Re from 17 Re due to the compression. This increases the magnetosheath field strength and in turn strengthens the magnetopause reconnection. The shock hasn't reached the nightside magnetosphere yet, and no shock impact

has been observed in this region. The strong earthward flow at 10:50 UT becomes weaker at 11:00 UT, indicating a low nightside reconnection rate.

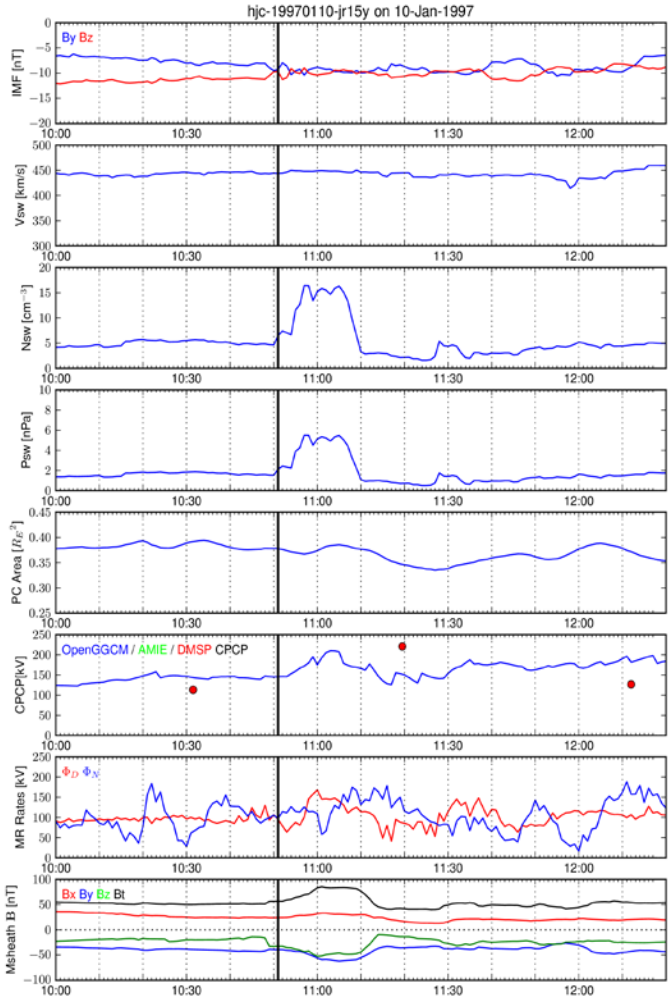

Figure 1. Solar wind conditions from OMNI (a-d) and the OpenGGCM-CTIM model results (e-h) on January 10, 1997. *The top four panels show IMF, solar wind plasma speed (Vsw), number density (Nsw), and dynamic pressure (Psw). The bottom four panels represents the DMSP observations, and the red/blue lines in the reconnection rate plot represent the dayside/nightside reconnection rates, respectively.*

The Psw shock reaches the near-Earth magnetotail at 11:10 UT, and convects to the further distant tail at 11:20 UT (See the third and fourth columns in Figure 2). After the shock completely flows away from the dayside magnetosphere, the bow shock expands up to Xgse = 24 Re at 11:20 UT, decreasing total magnetic field of the magnetosheath. This leads to weaker dayside reconnection. At the same time, the magnetotail is compressed due to the Psw shock. As a result, its magnetic fields are stretched along the Sun-Earth lines, and the Bx of both northern and southern magnetotail increases in opposite directions at 11:10 and 11:20 UT. This leads to

stronger anti-parallel reconnection near Xgse = -20 ~ -30 Re with fast earthward flows.

At 11:30 UT, the Psw shock flows away to the very distant magnetotail. As the near-Earth magnetotail expands, its magnetic fields decrease. The slow earthward plasma flow at Xgse= ~ -25 Re represents a reduced rate of nightside reconnection. On the other hand, the dayside magnetosphere re-adjust to a small Psw increase at 11:30 UT. The bow shock shrinks down to Xgse = 22 Re, and increase the magnetosheath fields and the dayside reconnection rates.

For the Jan 10, 1998 event, compression caused by the Psw shock increases magnetic fields near the magnetopause and the central plasma sheet, resulting in higher reconnection rates. Based on the third and fourth columns of Figure 2, the Psw shock takes about 10 minutes to move from the dayside to the nightside magnetosphere. This matches with 9 minutes of delay between the peaks of dayside and nightside reconnection rates.

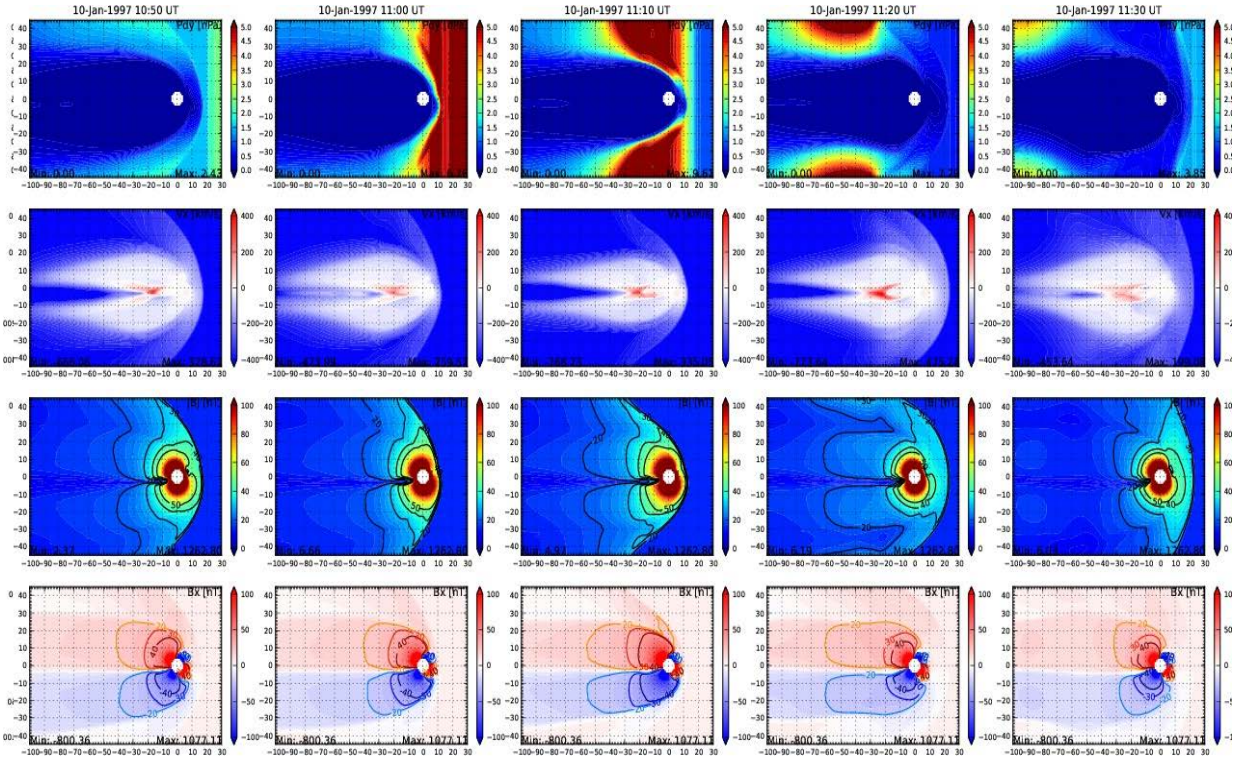

Figure 2. OpenGGCM-CTIM Magnetosphere plots on January 10, 1997. *The color contours indicates dynamic pressure (Pdy), Xgse component of plasma velocity (Vx), total magnetic field(Bt), and its Xgse component (Bx) on the noon-midnight meridian plane.*

3.2 30 April 1998

The second event of sudden Psw enhancement happens on Apr 30, 1998 while IMF By and Bz are nearly zero. The top four panels of Figure 3 show IMF, solar wind plasma speed, number density, and dynamic pressure obtained from WIND spacecraft. They are time-shifted to account for the solar wind propagation from the WIND location to the magnetopause nose. Solar wind dynamic pressure increases abruptly from 2 to 12 nPa at 09:25 UT, accompanied with fast and dense solar wind plasma. IMF generally directs to southwest for the first 2 hours of the Psw enhancement, and becomes northward and eastward after 11:30 UT. The major difference of this event from the previous one on Jan 10, 1997 is that Psw maintains its strength for several hours during relatively weak IMF.

We input the solar wind parameters into the OpenGGCM-CTIM model, and reproduce the magnetosphere-ionosphere responses to the Psw enhancement. The bottom four panels of Figure 2 show the modeled polar cap area, CPCP, reconnection rates, and magnetosheath magnetic fields, respectively. The blue line and red dots in the CPCP plot represents our model result and DMSP observations.

The modeled polar cap expands continuously during the first two hours of Psw enhancement. Most of the time, IMF is weakly southward. The compressed magnetosheath increases its magnetic fields and intensifies dayside reconnection. As this reconnection dominates over the nightside reconnection, the polar cap opens. At 11:30 UT, the polar cap starts closing due to the northward turning of IMF. The dayside reconnection becomes weaker, and the nightside reconnection plays a major role in the magnetosphere-ionosphere system. This lead to the polar cap closure.

Boudouridis et al. [2004b] have investigated the polar cap boundary motion of this event using the particle precipitation data of DMSP spacecraft. They investigated the poleward boundaries of auroral precipitation whenever DMSP satellites pass the polar regions. They focused on a total of 16 satellite crossings, and derived the polar cap boundaries before and after the Psw increase. Due to the poor data coverage on the dayside region, Boudouridis et al. [2004b] could not identify the dayside motion of polar cap boundary, but they found that the nightside boundary moves poleward after the Psw enhancement. This indicates the polar cap closure in the night zone.

The direct comparison between the model and observation is not easy with this polar cap

information. Boudouridis et al. [2004b] estimated the poleward boundary motion from a few data points observed at different times during 09:40 – 11:25 UT. Our model produces very complicate polar cap boundary, and this boundary continuously changes during the DMSP observation time. Although the one-to-one comparison is difficult, our model observes increase of the nightside reconnection rate during 9:25 – 9:50 UT and 10:20 – 10:45 UT. Thus, the nightside polar cap closes at least twice in the model, creating its poleward boundary motions during the DMSP observations. This can be interpreted as our model generates the ionospheric responses to a reasonable extent.

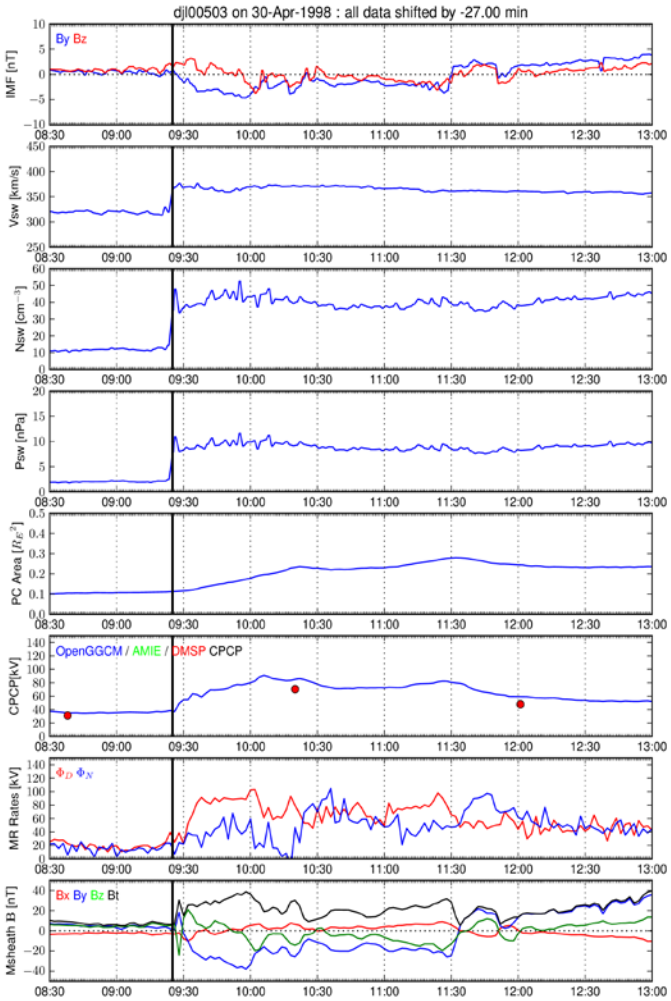

Figure 3. Solar wind conditions from WIND spacecraft (a-d) and the OpenGGCM-CTIM results (e-h) on April 30, 1998. *The solar wind data is time-shifted to propagate the solar wind from the WIND location to the magnetopause nose. See the descriptions in Figure 1 for more details of this figure.*

While the polar cap boundary motions are difficult to compare, CPCP clearly shows a good agreement between the model results and DMSP observations. The modeled CPCP begins to increase when the initial pressure front hits the magnetosphere. It reaches its maximum at ~ 10:05 UT, and then slowly decreases for the next several hours. The DMSP observations show a similar pattern. CPCP increases from 35 to 70 kV about an hour after the Psw enhancement, and decreases to 50 kV at 12:00 UT. The CPCP magnitudes also match well with the model results.

Figure 3.g shows the reconnection rates calculated from OpenGGCM-CTIM. The dayside reconnection rate increases from 20 UT to 90 kV in 30 minutes after the Psw shock. Then, it generally decreases for the next three hours. The dayside rate is highly correlated to the total magnetosheath field (black line) in Figure 3.h, although we calculate the reconnection rate separately from the fields. This supports the empirical reconnection models [references] assuming that the magnetopause reconnection rate is linearly related to the magnetosheath fields.

The nightside reconnection rate shows more complicate responses to the Psw enhancement. It slowly reaches its first maximum at 09:50 UT, about 25 minutes after the shock arrival at the magnetopause nose. Then, it repeats the increase and decrease patterns twice with the peaks at 10:40 and 11:45 UT. To understand the reconnection mechanisms on the nightside region, we plot the magnetosphere on the noon-midnight meridian plane in Figure 4. It shows dynamic pressure (ρv^2), plasma pressure (nkT), X component of velocity (Vx), and X component of magnetic field (Bx) at different times of this event.

At 09:24 UT, the Psw shock front is not yet arrived on the dayside magnetopause. We observe the preexisting reconnection near X= -18 Re with fast plasma flows in opposite directions. The Psw front moves to the near-earth magnetotail at 09:38 UT. The plasma velocity becomes weak, and the previous reconnection disappears. Note that the green region of plasma pressure moves to a distant tail. The central plasma sheet stretches tailward due to the Psw compression, and as a result, the magnetic field Bx becomes strong in both the northern and southern magnetotail. At 09:54 UT, the Psw convects to further distant tail, compressing the broad region of the magnetotail. The increased Bx initiates anti-parallel reconnection near X=-27 Re, creating fast sunward flows.

After the Psw enhancement takes over the entire magnetotail, the nightside magnetosphere reacts as normal. The solar wind plasma continuously enters into the magnetosphere through strong dayside reconnection, and piled up on the magnetotail. A

plasmoid structure builds up near X=-25 RE at 10:10 UT, and the nightside magnetosphere becomes thick and dense at 11:08UT (See the plasma pressure plots of the corresponding times in Figure 4). As the magnetosheath field Bz turns northward at 10:28 and 11:35 UT, the dayside reconnection weakens and the nightside reconnection predominates. As a result, the solar wind plasma piled at the magnetotail moves back to the Earth's geospace system with strong earthward flows at 10:28 and 11:38 UT.

The magnetotail compression due to the Psw enhancement results in the first peak of nightside reconnection rate at 09:50 UT. As the Psw maintains its strength for several hours, the magnetotail moves back as normal, and repeats its loading-unloading process. This creates the other peaks of nightside reconnection rate at 10:28 and 11:35 UT. This indicates that the Earth's geospace reacts to the Psw effect at least for an hour.

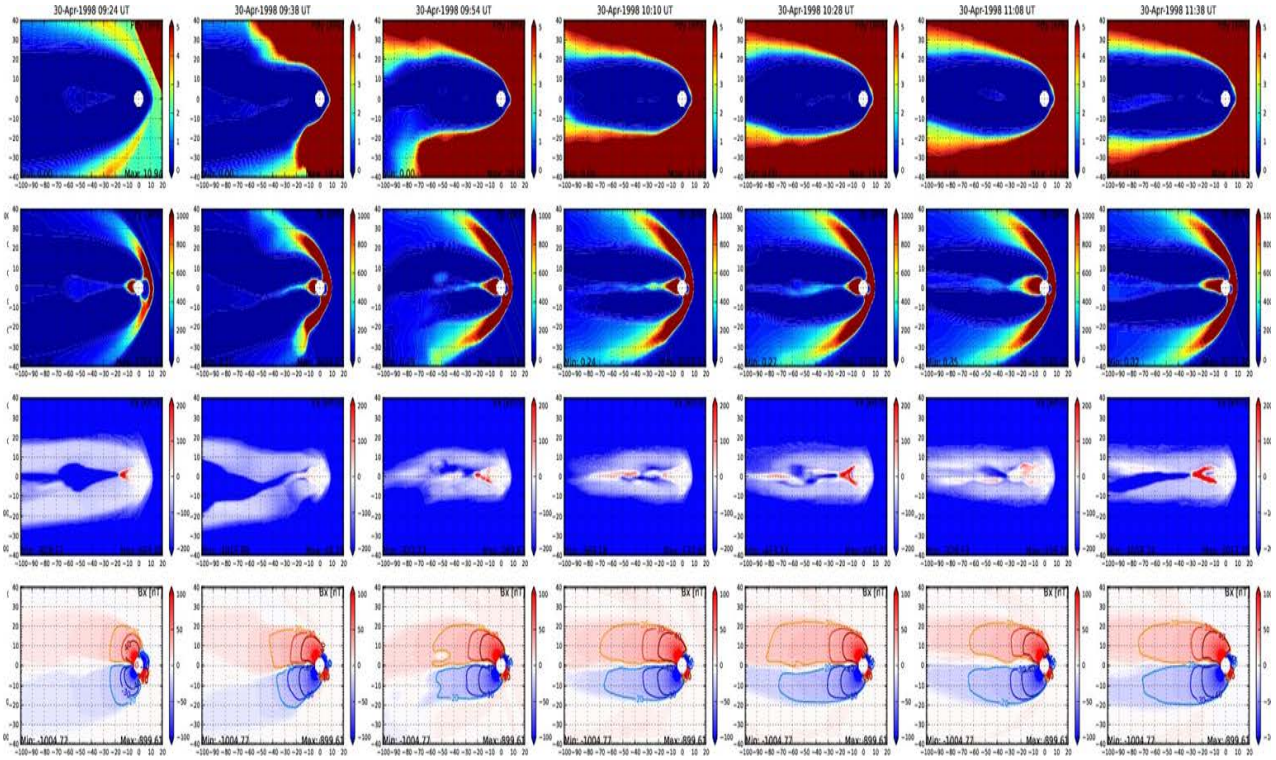

Figure 4. OpenGGCM-CTIM Magnetosphere plots on April 30, 1998. *The color contours represent the dynamic pressure (Pdy), plasma pressure (Pp), Xgse component of plasma velocity (Vx), and Xgse component of magnetic fields (Bx) on the noon-midnight meridian.*

3.3 12 October 2000

The last event happens on Oct 12 2000 during northward IMF. The top four panels of Figure 5 show IMF, solar wind speed, number density, and dynamic pressure observed from Geotail spacecraft. At 22:29 UT, Psw jumps from 1 to 5 nPa with increase of solar wind number density and speed. The enhanced Psw is sustained for several hours while IMF directs to northeast in general. We introduce the solar wind conditions to the OpenGGCM-CTIM, and calculates the polar cap area, CPCP, reconnection rates, and magnetosheath magnetic fields of this event. The results are shown in the bottom four panels of Figure 5.

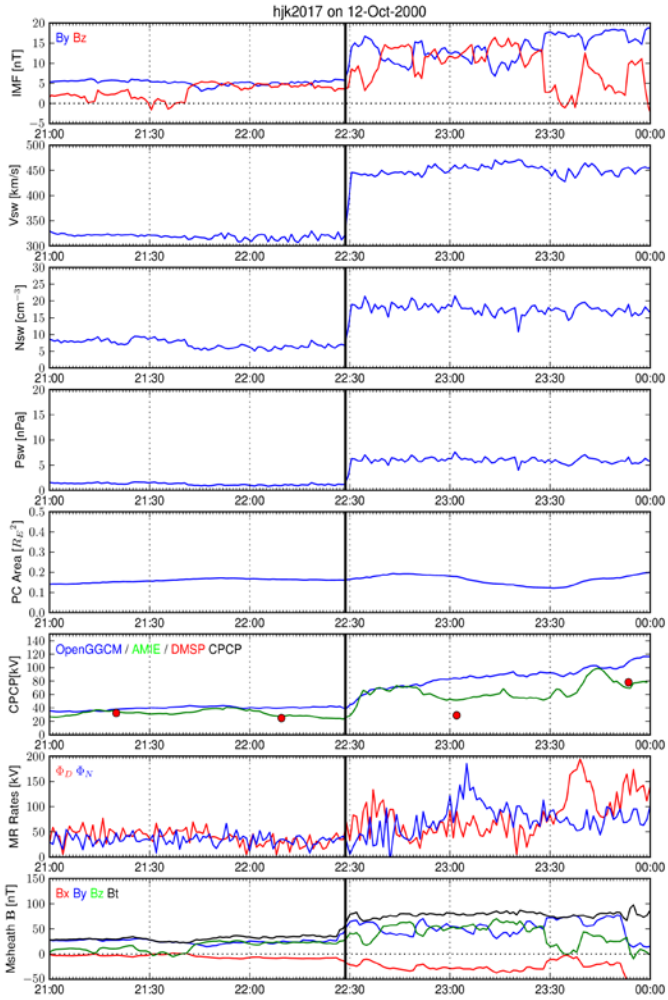

Figure 5. Solar wind conditions from Geotail spacecraft (a-d) and the OpenGGCM-CTIM results (e-h) on October 12, 2000. *The green line in the CPCP plot represents the AMIE predictions. See the descriptions in Figure 1 for more details.*

As the Psw front approaches, the magnetosheath is compressed and its magnetic fields intensify. The magnetopause reconnection becomes stronger due to this field change, and reaches its maximum rate at 22:37 UT. During this period, the dayside reconnection predominates the nightside one, resulting in the polar cap expansion. The nightside reconnection reacts later due to the solar wind propagation time from the magnetopause to the magnetotail. It reaches its first peak at ~22:40 UT, about 15 minutes after the shock arrival at the magnetopause. This reconnection rate excels the dayside rate at ~ 22:45 UT, and reaches its second peak at 23:05 UT. The polar cap area continuously shrinks due to the strong nightside reconnection from 22:45 to 23:35 UT until the magnetosheath field becomes slightly southward.

For the model validation, we compare CPCPs from OpenGGCM-CTIM, DMSP, and Assimilative Mapping of Ionospheric Electrodynamics (AMIE). The red dots, yellow and blue lines in Figure 5.f represent DMSP observations, AMIE predictions, and our model results, respectively. The modeled CPCP jumps from 36 to 70 kV in a few minutes after the Psw enhancement, and slowly increases for the rest period. DMSP spacecraft observe the CPCP increase at 23:50 UT, but not at 23:02 UT. The DMSP orbit at this time does not cross the center of ionospheric convection cells, measuring a low CPCP.

To cover the poor DMSP data, we uses CPCP predicted from the AMIE procedure [Richmond and Kamide, 1988]. AMIE assimilates observations from radar, ground magnetometer, and low-orbiting satellites to estimate the entire ionospheric electrodynamics such as electric potentials, conductances, and currents. The typical uncertainty of AMIE electric field map is 50% or less, and can go down to 30% during the interval of good data coverage [Knipp and Emery, 1997]. The AMIE CPCP rises up to 70 kV in a few minutes after the Psw enhancement. Then, it decreases to 50 kV during 22:45~ 23:40 UT, and jumps up again to100 kV at 23:40 UT. Although our model does not generate the CPCP decrease, its magnitude and increase patterns at the Psw arrival generally matches with AMIE.

Unlike the previous events, the dayside reconnection rate of this event is weakly correlated to the magnetosheath field strength. The total magnetic field jumps from 30 to 70 nT at the arrival of Psw front. In a response to this change, the reconnection rate increases up to 120 kV at 22:40 UT. However, the rate soon reduces and stays at ~ 55 kV while the magnetosheath field maintain its strength more than an hour. This is because the dayside magnetosphere reaches an equilibrium status due to the steady magnetosheath field magnitude. This is different from the

previous events that the magnetosheath fields continuously vary. The dayside magnetosphere adjusts to the field change, altering its reconnection rate without a time to reach equilibrium. Therefore, the previous events show a high correlation between the magnetosheath field and reconnection rate.

To understand the nightside reconnection mechanisms, Figure 6 shows the magnetosphere on the noon-midnight plane during 22:30 – 23:10 UT. Dynamic pressure, plasma pressure, X component of velocity, and X component of magnetic field are plotted in each row. At 22:30 UT, the Psw enhancement hits the dayside magnetosphere, and haven't reached the magnetotail yet. The nightside magnetosphere is quiet without strong plasma flows. As the Psw front arrives the near-Earth tail at 22:40, the compressed magnetotail is stretched along the Sun-Earth line, increasing the Bx in opposite directions and initiating strong anti-parallel reconnection near X= -30 Re with fast earthward flows. The nightside reconnection weakens at 22:50 and 23:00 UT with slower earthward flows. However, the Psw enhancement continuously compresses the magnetotail as it propagates further tailward. This increases magnetic field Bx in both northern and southern magnetotail, generating strong magnetic reconnection at 23:10 UT. Thus, the Psw enhancement of this event compresses the magnetotail strong enough to create two peaks of reconnection rate.

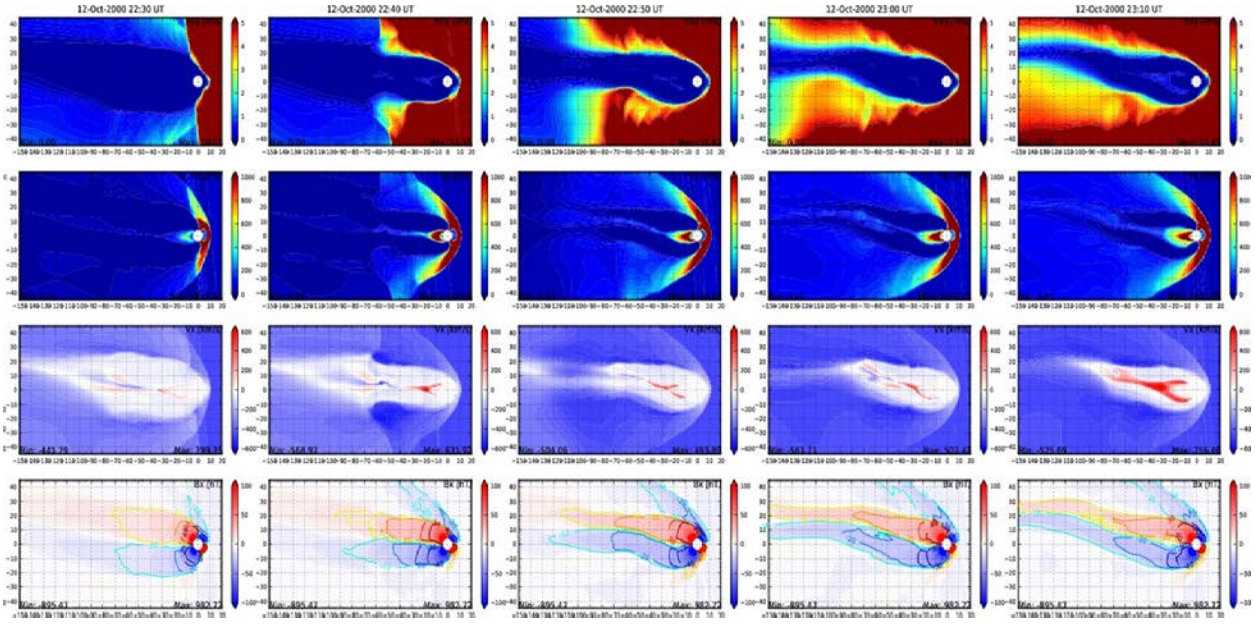

Figure 6. OpenGGCM-CTIM Magnetosphere plots on October 12, 2000. *See the description in Figure 4 for more details.*

4. DISCUSSION

In order to understand the MI coupling dynamics during the sudden enhancement of solar wind dynamic pressure, we select three unique events happened during negative, near-zero, and positive IMF Bz. We simulate their MI responses to the Psw increase using OpenGGCM-CTIM model. Our model results generally matches with the previous observational studies on these events. The OpenGGCM-CTIM specifically reproduces increase of cross-polar-cap-potential, a well-known MI response to the Psw enhancement. The magnitude and jump scale of CPCP is comparable to the DMSP observations and the AMIE prediction. In this section, we discuss how dayside and nightside reconnection behaves throughout the Psw increase. Then, we focus on the relative importance of each merging rate on the CPCP increase, i.e., ionospheric convection enhancements.

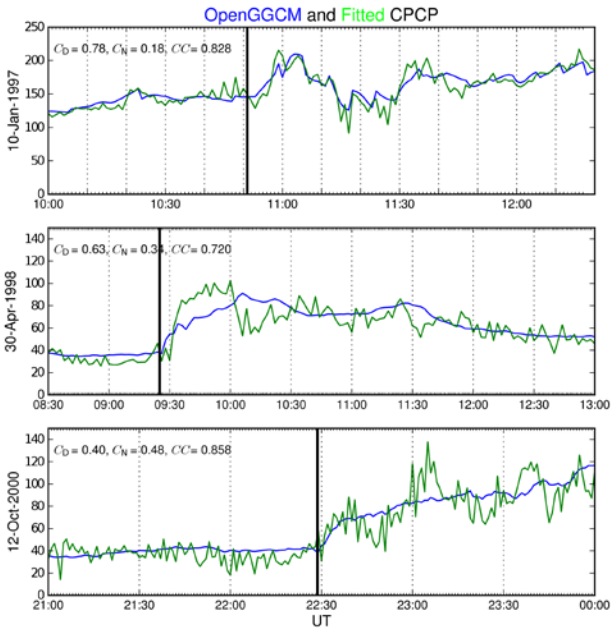

Figure 7. CPCP fitting results of the three events. *The blue and green lines represent the OpenGGCM CPCP and the fitted CPCP (= Cd Φd + Cn Φn + Φv), respectively. The upper right conner of each panel shows the dayside/nightside regression coefficients (Cd/Cn) and the correlation coefficients (CC) between the modeled and fitted CPCPs.*

4.1 Reconnection patterns during the sudden Psw enhancement

We employed the OpenGGCM-CTIM model to simulate the MI responses of three unique events which happen during negative, near-zero, and positive IMF Bz. Our model reproduced CPCP increase for all three events, and the CPCP magnitude and patterns matches to a reasonable extent with the DMSP observations and AMIE predictions.

Dayside reconnection reacts first to the Psw enhancements, increasing its rate to a maximum value in a few minutes after the arrival of Psw increase. Nightside reconnection responds to the Psw increase about 10-15 minutes later due to the solar wind propagation from the magnetopause nose to the magnetotail. Boudouridis et al. [2011] have shown from one event study that the nightside ionospheric flows rise about 10-15 minutes after the Psw shock arrival. This agrees with our modeling results.

The dayside reconnection rate increases due to the magnetosheath compression by Psw enhancement. This compression strengthens magnetic fields in the magnetosheath. The stronger magnetosheath fields initiates intense anti-parallel reconnection on the dayside magnetopause, thus increasing its reconnection rate. For Jan 10, 1997 and Apr 30, 1998, this rate is highly correlated with the magnetosheath field strength, supporting this idea. Note that the empirical models of dayside reconnection assumes a linear relation of the magnetosheath field to a reconnection rate. Our study calculates the reconnection rates based only on the open flux changes across the dayside OCB, not a magneotsheath field. However, the patterns of magnetisheath field strength and the dayside reconnection match pretty well, demonstrating the assumption of empirical models.

Unlike the first two events, the Oct 12 2000 event does not show a good correlation between the magnetosheath fields and the reconnection rates. The magnetosheath fields in the first two events continuously changes, and therefore the dayside magnetosphere reacts to the new conditions without time to reach equilibrium. The dayside reconnection rate continuously varies according to the change of magnetosheath fields. On the other hand, for the OCT 12 2000 event, the magnetosheath field remains steady for several hours after it increases at the arrival of Psw enhancements. The dayside reconnection rate responses to the intensified magnetosheath fields at the beginning of Psw enhancement, but soon reduces although the magnetosheath field stays high. This is because the dayside magnetosphere reaches to equilibrium with the prolonged field strength.

Nightside reconnection also intensifies as the Psw enhancement compresses the magnetotail. The magnetic field Bx near the central plasma sheet intensifies in opposite directions, resulting in active anti-parallel reconnection with fast earthward flows. Because of solar wind propagation from the dayside to nightside magnetosphere, the compression effect on Φ_n appears 10 – 20 minutes after Φ_d reaches maximum.

This compression impact on the magnetotail is observed for all three event studies, but after this impact, the nightside magnetosphere behaves differently at each case. On Jan 10 1997, the magnetotail experiences another compression due to the next, relatively small Psw increase, which in turn initiates small increase of the nightside reconnection rate. For the Apr 30, 1998 event, the nightside magnetosphere repeats the loading-unloading process as the strong dayside reconnection piles up the solar wind plasma. The magnetotail on Oct 12 2000 experiences the compression by Psw enhancement again at the distant tail. Due to the steady magnetosheath fields, the nightside magnetosphere remains clean from any dayside driving, and as a results the Psw compression effect observes twice at near and distant tail locations.

4.2 Relation between the reconnection rates and the ionospheric convection

We apply multiple linear regression method to fit our model results to the function $CPCP = C_D \Phi_D + C_N \Phi_N + viscosity$. The C_D and C_N are regression coefficients of dayside and nightside reconnection rates (Φ_D and Φ_N). They can be considered as a weight factor determining which fraction of the corresponding reconnection contributes to the CPCP enhancements. Figure 7 shows the fitting results (green lines) with the OpenGGCM-CTIM CPCPs (blue lines) for all three events. The black vertical lines indicate when the Psw enhancement arrives at the magnetopause nose. On the upper left conner are shown the regression coefficients (C_D and C_N) and correlation coefficient (CC) between the modeled and fitted CPCPs. The CC values of three events are 0.828, 0.720, and 0.858, indicating that the CPCP fit function follows the modeled CPCP behavior pretty well.

The first events on Jan 10, 1997 happens during strongly southward IMF. Its dayside reconnection coefficient (C_D) is 0.78, about four times stronger than the nightside one at 0.18. The second event on Apr 30, 1998 happens while IMF Bz is weakly southward for the most time of Psw enhancement. Its dayside coefficient becomes weaker but still two times higher than the nightside one. This indicates that dayside reconnection significantly control the CPCP during

strong Psw and southward IMF. The last event on Oct 12, 2000 occurs during northward IMF, observing a stronger nightside correlation coefficient. Thus, the nightside reconnection dominates the CPCP enhancement during northward IMF.

To investigate why the contribution patterns vary according to IMF conditions, we plot the ionosphere convection patterns before and after the Psw shock for all three events in the left and right columns of Figure 8. Color contours, arrows, and thick black lines represent electric potentials, plasma flows, and OCB of the northern ionosphere, respectively. All events are shown from top to bottom. Our model observes that the ionospheric potentials and plasma flow intensify after the Psw increase.

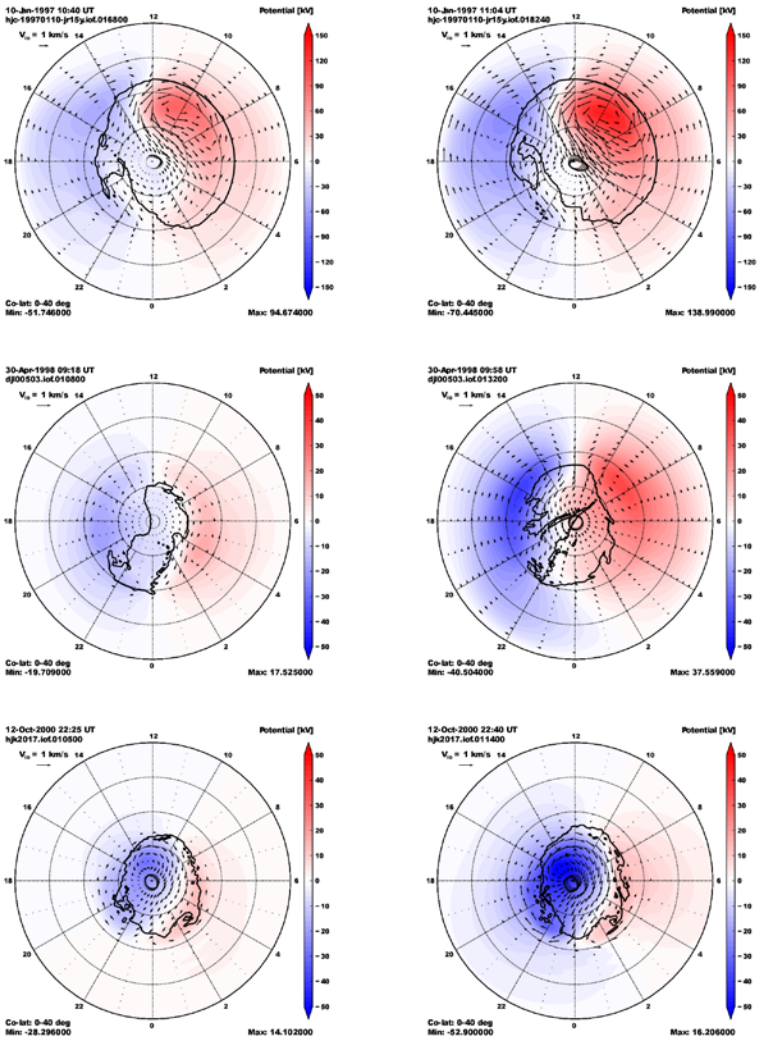

Figure 8. OpenGGCM-CTIM ionosphere before and after the Psw enhancements. *The top to bottom panels show the ionospheric conditions on January 10, 1997, Apr 30 1998, and October 20, 2000, respectively. The color contour displays the ionosphere electric potential. The thick black lines and arrows*

represent the open closed field line boundary and ionospheric plasma convections.

For strongly and weakly southward IMF, we observe two cell convection patterns (See the top two panels of Figure 8). After strong Psw arrives at the Earth's magnetosphere, dayside reconnection significantly increases, creating strong anti-sunward plasma flows across the polar cap region. We observe the enhanced flows directing from 14 to 02 MLT for the Jan 10 1997 event and from 12 to 20 MLT for the Apr 30 1998 event. These ionospheric flows create the dawn-to-dusk electric fields and intensifie the preexisting electric potential patterns, which in turn leads to the CPCP increase.

For northward and eastward IMF, the high-latitude magnetopause reconnection appears on the duskside. As the kinked open field lines moves sunward due to the magnetic tension force, the ionospheric flows convect sunward in the 12-17 MLT region with the field lines (See the bottom panels of Figure 8). As the tension force becomes weaker, the magnetosheath flow direction plays a major role to convect the open field lines, creating anti-sunward flow on the dawnside magnetosphere. Note that the dayside reconnection leads to both sunward and anti-sunward ionospheric flows. The former create the dusk-to-dawn electric fields opposite to the general ionospheric field direction, weakening the ionospheric potentials. On the other hand, the latter generates the electric field in a dawn-to-dusk direction, strengthening the potentials. The opposite flow behaviors leads to a less contribution of dayside reconnection on the CPCP.

Whether electric fields control the ionospheric plasma flows, or the flow controls electric fields are not the point of this study.

5. SUMMARY

We investigated where, when, how solar wind energy flows into the magnetosphere-ionosphere system during sudden enhancements of solar wind dynamic pressure. We specifically focused on the behaviors of dayside and nightside reconnection as well as their relative importance on ionospheric convection enhancements in terms of CPCP. From the detailed modeling analysis, we found that:

1. Dayside reconnection reacts directly to the Psw enhancements, reaching its maximum rate in a few minutes. The magnetosheath compression due to the Psw increase intensifies the

magnetosheath field strength, initiating stronger anti-parallel reconnection on the magnetopause.

2. Nightside reconnection rate reaches its maximum about 10 – 20 minutes after the maximum dayside rate. This delay is caused by solar wind propagation from the dayside magnetopause to the nightside magnetosphere. The Psw increase compresses the magnetotail, increasing magnetic field Bx of northern and southern magnetosphere in opposite directions. This intensifies the anti-parallel reconnection near the central plasma sheet.

3. For southward IMF, we observed that dayside reconnection contributes to CPCP twice to four times more than the nightside reconnection. On the other hand, for northward IMF, dayside contribution becomes weaker. The high latitude magnetopause reconnection produces sunward ionospheric flows, creating the dusk-to-dawn electric field and weakening the dawn-to-dusk electric field. This leads to a weaker dayside contribution on CPCP.

4. The ECP model assumes a linear relation between CPCP and reconnection rates. However, the contribution coefficient of dayside reconnection varies, depending on magnetopause reconnection geometry. Thus, the coefficient behaves non-linearly, brings up the need of a new alternative model to explain the non-linear system.

REFERENCES

Blanchard, G. T., L. R. Lyons, O. de La Beaujadiere, R. A. Doe, and M. Mendillo, (1996), Measurements of the magnetotail reconnection rate, J. Geophys. Res., 101, 15,265.

Borovsky, J. E., M. Hesse, J. Birn, and M. M. Kuznetsova, (2008), What determines the reconnection rate at the dayside magnetosphere?, J. Geophys. Res., 113, A07210, doi:10.1029/2007JA012645.

Boudouridis, A., E. Zesta, L. R. Lyons, P. C. Anderson, and D. Lummerzheim, (2003), Effect of solar wind pressure pulses on the size and strength of the auroral oval, J. Geophys. Res., 108(A4), 8012, doi:10.1029/2002JA009373.

Boudouridis, A., E. Zesta, L. R. Lyons, P. C. Anderson, and D. Lummerzheim, (2004a), Magnetospheric reconnection driven by solar wind pressure fronts, Ann. Geophys., 22, pp. 1367-1378.

Boudouridis, A., E. Zesta, L. R. Lyons, and P. C. Anderson, (2004b), Evaluation of the Hill-Siscoe transpolar potential saturation model during a solar wind dynamic pressure pulse, Geophys. Res. Lett., 31, L23802, doi:10.1029/2004GL021252.

Boudouridis, A., E. Zesta, L. R. Lyons, P. C. Anderson, and D. Lummerzheim, (2005), Enhanced solar wind geoeffectiveness after a sudden increase in dynamic pressure during southward IMF orientation, J. Geophys. Res., 110, A05214, doi:10.1029/2004JA010704.

Boudouridis, A., L. R. Lyons, E. Zesta, and J. M. Ruohoniemi, (2007), Dayside reconnection enhancement resulting from a solar wind dynamic pressure increase, J. Geophys. Res., 112, A06201, doi:10.1029/2006JA012141.

Boudouridis, A., E. Zesta, L. R. Lyons, P. C. Anderson, and A. J. Ridley, (2008a), Temporal evolution of the transpolar potential after a sharp enhancement in solar wind dynamic pressure, Geophys. Res. Lett., 35, L02101, doi:10.1029/2007GL031766.

Boudouridis, A., L. R. Lyons, E. Zesta, J. M. Ruohoniemi, and D. Lummerzheim, (2008b), Nightside flow enhancement associated with solar wind dynamic pressure driven reconnection, J. Geophys. Res., 113, A12211, doi:10.1029/2008JA013489.

Boudouridis, A., L. R. Lyons, E. Zesta, J. M. Weygand, A. J. Ribeiro, and J. M. Ruohoniemi, (2011), Statistical study of the effect of solar wind dynamic pressure fronts on the dayside and nightside ionospheric convection, J. Geophys. Res., 116, A10233, doi:10.1029/2011JA016582.

De La Beaujardiere, O., L. R. Lyons, and E. Friis-Christensen, (1991), Sondrestrom radar measurements of the reconnection electric field, J. Geophys. Res., 96, 13,907.

Fuller-Rowell, T. J., D. Rees, S. Quegan, R. J. Moffett, M. V. Codrescu, and G. H. Millward, (1996), A coupled thermosphere - ionosphere model (CTIM), in STEP Report, edited by R. W. Schunk, p. 217, NOAA/NGDC, Boulder, Colorado, Scientific Committee on Solar Terrestrial Physics (SCOSTEP).

Hubert, B., M. Palmroth, T. V. Laitinen, P. Janhunen, S. E. Milan, A. Grocott, S. W. H. Cowley, T. Pulkkinen, and J.-C. G´erard, (2006), Compression of the Earth's magnetotail by interplanetary shocks directly drives transient magnetic flux closure, Geophys. Res. Lett., 33, L10105, doi:10.1029/2006GL026008.

Hubert, B., C. Blockx, S. E. Milan, and S. W. H. Cowley, (2009), Statistical properties of flux closure induced by solar wind dynamic pressure fronts, J. Geophys. Res., 114, A07211, doi:10.1029/2008JA013813.

Knipp, D. J. and B. A. Emery, (1997), Mapping ionospheric substorm response, Adv. Space Res., 20, No 4/5, pp. 895-905.

Lockwood, M., M. Hairston, I. Finch, and A. Rouillard, (2009), Transpolar voltage and polar cap flux during the substorm cycle and steady convection events, J. Geophys. Res., A01210, doi:10.1029/2008JA013697.

Lyons, L. R., E. Zesta, J. C. Samson, and G. D. Reeves, (2000), Auroral disturbances during the January 10, 1997 magnetic storm, Geophys., Res., Lett., 27, 3237.

Milan, S. E., S. W. H. Cowley, M. Lester, D. M. Wright, J. A. Slavin, M. Fillingim, C. W. Carlson, and H. J. Singer, (2004), Response of the magnetotail to changes in the open flux content of the magnetosphere, J. Geophys. Res., 109, A04220, doi:10.1029/2003JA010350.

Ober, D. M., N. C. Maynard, W. J. Burke, W. K. Peterson, J. B. Sigwarth, L. A. Frank, J. D. Scudder, W. J. Hughes, and C. T. Russell, (2001), Electrodynamics of the poleward auroral border observed by Polar during a substorm on April 22, 1998, J. Geophys. Res., 106(A4), 5927.

Ober, D. M., G. R. Wilson, W. J. Burke, N. C. Maynard, and K. D. Siebert, (2007), Magnetohydrodynamic simulations of transient transpolar potential responses to solar wind density changes, J. Geophys. Res., 112, A10212, doi:10.1029/2006JA012169.

Raeder, J., Y. Wang, and T. Fuller-Rowell, (2001), Geomagnetic Storm Simulation With a Coupled Magnetosphere-Ionosphere-Thermosphere Model, in: Space Weather: Progress and Challenges in Research and Applications, Geophysical Monograph 125, in: pp. 377-384, editor(s): P. Song, H. J. Singer, and G. Siscoe, Publisher: AGU, Washington D.C.

Raeder, J., (2003), Global Magnetohydrodynamics – A Tutorial, in: Space Plasma Simulation, editor(s): J. Buechner, C. T. Dum, and M. Scholer, Lecture Notes in Physics, 615, Publisher: Springer Verlag, Heidelberg, ISBN 3-540-00698-2.

Raeder, J., D. Larson, W. Li, E. L. Kepko, and T. Fuller-Rowell, (2008), OpenGGCM simulations for the THEMIS mission, Space Science Reviews, 141, pp. 535-555, doi:10.1007/s11214-0421-5.

Zesta, E., H. J. Singer, D. Lummerzheim, C. T. Russell, L. R. Lyons, and M. J. Brittnacher, (2000), The effect of the January 10, 1997, pressure pulse on the magnetosphere-ionosphere current system, in Magnetospheric Current Systems, Geophys. Monogr. Ser., vol. 118, edited by S. Ohtani et al., pp. 217–226, AGU, Washington, D. C.

DISTRIBUTION LIST

DTIC/OCP
8725 John J. Kingman Rd, Suite 0944
Ft Belvoir, VA 22060-6218 1 cy

AFRL/RVIL
Kirtland AFB, NM 87117-5776 2 cys

Official Record Copy
AFRL/RVBXI/Dr. Daniel Ober 1 cy

This page is intentionally left blank.